

# Fine structures in the spectrum of the open-boundary Heisenberg XXZ chain at large anisotropies

Auditya Sharma

*International Institute of Physics - Federal University of Rio Grande do Norte, Natal, RN, Brazil*

Masudul Haque

*Max-Planck Institute for the Physics of Complex Systems, Nöthnitzer Str. 38, 01187 Dresden, Germany*

At large anisotropies, the spectrum of the Heisenberg XXZ spin chain separates into ‘bands’ with energies largely determined by the number of domain walls. The band structure is richer with open boundary conditions: there are more bands and the bands develop intricate fine structures. We characterize and explain these structures and substructures in the open-boundary chain. The fine structures are explained using degenerate perturbation theory. We also present some dynamical consequences of these sub-band structures, through explicit time evolution of the wavefunction from initial states motivated by the fine structure analysis.

## I. INTRODUCTION

Traditionally, the theory of many-body quantum systems has focused on the ground state and low-energy parts of the eigenspectrum. This is well-justified in solid-state systems which are usually in contact with a thermal bath and typically relax fast to low-energy sectors. As a result, parts of the many-body eigenspectra away from the low-energy sector were generally considered to be of no interest, for much of the history of condensed matter physics.

In recent years, the perspective has changed due to the advent of new experimental setups, particularly those employing cold atom gases, which have promoted the study of non-equilibrium situations in *isolated* quantum systems. In an isolated situation, energy conservation ensures that a system with an initially high energy will not reach the low-energy parts of the spectrum; the low-energy sector may thus be unimportant. This provides topical motivation to understand aspects of the full spectra of many-body systems. In particular, spectral structures in previously less-explored spectral regions can give rise to unexpected dynamical phenomena.

In this work, we report and explain fine structures present in the eigenspectrum of the anisotropic Heisenberg (XXZ) chain with open boundary conditions. These spectral features are related to the binding of magnons and the spatial relationship of bound multi-magnons with the edges of the open chain. Some related spectral fine structures were studied briefly in Ref. [1], where it was also found that these structures give rise to unexpected dynamics suppression phenomena (‘edge-locking’ of bound multi-magnons). The study of this class of dynamics is now particularly important because of the remarkable recent success in constructing spin chains in a cold-atom setup [2, 3], which promises near-future experimental explorations of many types of time evolution experiments with finite-size spin chains.

The XXZ chain is a fundamental model of condensed matter physics, and has long been the subject of sustained theoretical activity. The open chain has received

less detailed attention than the periodic case. The Hamiltonian describing the system is

$$H_{XXZ} = J_x \sum_j [S_j^x S_{j+1}^x + S_j^y S_{j+1}^y + \Delta S_j^z S_{j+1}^z] \quad (1)$$

For an  $L$ -site chain, the summation runs from  $j = 1$  to  $j = L - 1$  with open boundary conditions, and runs from  $j = 1$  to  $j = L$  with periodic boundary conditions, the site  $L + 1$  being identified with site  $j = 1$ .

The  $S^z S^z$  term acts as an ‘interaction’ penalizing alignment of neighboring spins. The in-plane terms  $(S_j^x S_{j+1}^x + S_j^y S_{j+1}^y) = \frac{1}{2}(S_j^+ S_{j+1}^- + S_j^- S_{j+1}^+)$  provide ‘hopping’ processes. Since  $H_{XXZ}$  preserves total  $S^z$ , the dynamics is always confined to sectors of fixed numbers  $N_\uparrow$  of up-spins. For simplicity, our description will sometimes focus on small  $N_\uparrow$ , i.e., highly polarized spin chains. However, much of the phenomena described here is also valid at smaller magnetization (larger  $N_\uparrow$ ). We will mostly consider the large  $\Delta$  regime, where the spectral structures are most prominent. Unless otherwise specified, energy and time are measured in units of  $J_x$  and  $\hbar/J_x$  respectively.

Refs. [2, 3] have experimentally realized the XXZ chain Hamiltonian (1) with  $\Delta \approx 1$  using two hyperfine states of a bosonic species in a Mott phase. Ref. [3] has also explored the propagation of bound multi-magnons, of particular relevance to the physics described in the present manuscript. A setup suitable for realizing large  $\Delta$  values is currently under development [4]. In addition, the XXZ model has been shown to describe Josephson junction arrays of the flux qubit type [5], and may also be realizable in optical lattices [6] or with polaritons in coupled arrays of cavities [7]. It should be possible to explore the spectral structures and associated dynamical phenomena described in the present article in one of these settings in the foreseeable future.

At large  $\Delta$ , the number of domain walls (bonds connecting oppositely pointing spins) is a good indicator of energy, and the spectrum accordingly splits up into energetically separated groups of eigenstates or ‘bands’. Section II describes this gross ‘band’ structure and the differ-

ence between open and periodic chains. As pointed out in Ref. [1], the open chain spectrum not only has more bands than the periodic chain spectrum, but each of the bands also has intricate sub-structures. Ref. [1] studied the top two bands and dynamical phenomena associated with them. This is briefly reviewed in Section III. The main object of this paper is to describe and explain the substructures in the larger bands lower in the spectrum. In Sections IV and VI, we explain the main sub-band structures within the third and fourth bands from the top. Section V presents real-time evolution results which highlight the internal structure of the third band.

## II. ‘BAND’ STRUCTURE IN MANY-BODY SPECTRUM

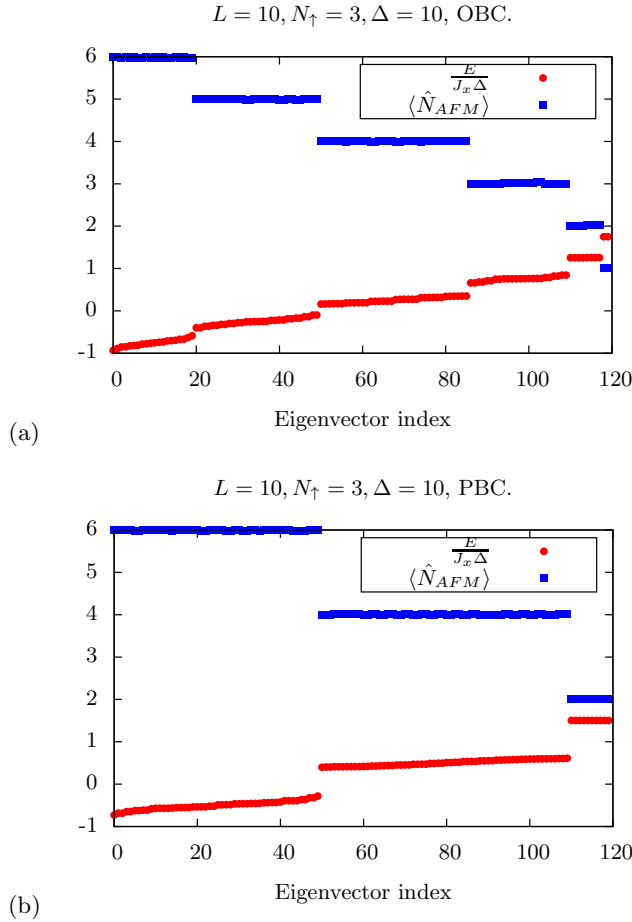


FIG. 1. Energy and  $\langle \hat{N}_{AFM} \rangle$  (average number of bonds connecting antiferromagnetically aligned spins) of eigenstates plotted against eigenstate index, for (a) open boundary conditions, and (b) periodic boundary conditions. We restrict to the  $N_{\uparrow} = 3$ -sector, for a  $L = 10$  (10-site) chain at large anisotropy  $\Delta = 10$ . There are 6 bands in the OBC spectrum and only 3 bands in the PBC spectrum.

For  $\Delta = \infty$ , the spectrum splits into bands, because

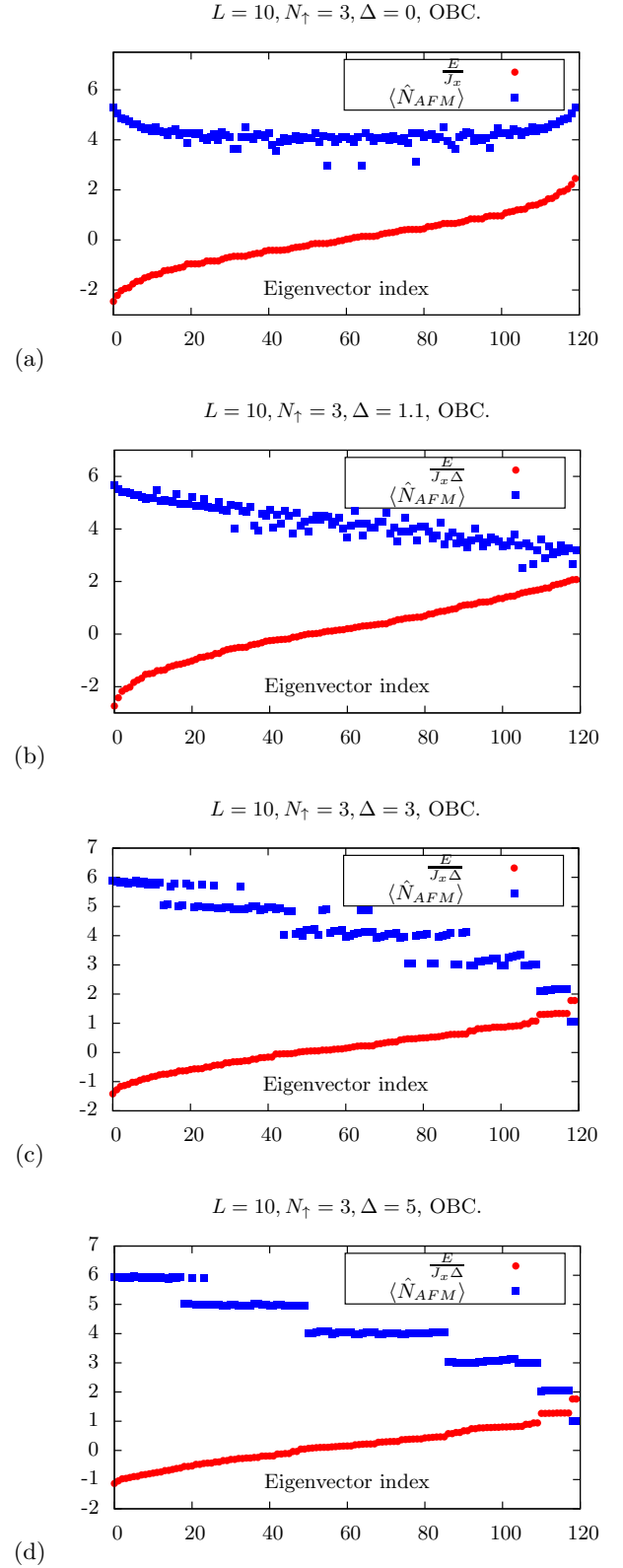


FIG. 2. Energy and  $\langle \hat{N}_{AFM} \rangle$  of eigenstates plotted against eigenvector index with open boundary conditions for several  $\Delta$  values. The bands in energy start appearing at high  $\Delta$ ; at moderate  $\Delta$  the band structure is slightly easier to see through the jumps in  $\langle \hat{N}_{AFM} \rangle$ .

the Hamiltonian becomes further block diagonal. The number of bands is easily understood from simple combinatorics. In this limit, the in-plane terms in the Hamiltonian can be neglected, and we see a grouping of states into blocks that have different numbers of ‘anti-ferromagnetic nearest neighbors’,  $N_{AFM}$ . The quantity  $N_{AFM}$  can be defined as an operator, which acts on a state  $|\phi\rangle$  in the  $S_z$  basis (thus having a diagonal representation in the  $S_z$  basis) as

$$\left(\sum_j S_j^z S_{j+1}^z\right) |\phi\rangle = N_{AFM} |\phi\rangle, \quad (2)$$

where  $N_{AFM}$  is the number of nearest-neighbors that have opposite spins. Clearly this quantity depends on the type of boundary condition in place (as evident from the operator definition above, where  $j$  accepts the value  $L$  only for periodic boundary conditions). For example, the state  $|\uparrow\uparrow\uparrow\downarrow\downarrow\cdots\downarrow\rangle$  has  $N_{AFM} = 2$  for periodic boundary conditions, but it is only  $N_{AFM} = 1$  for open boundary conditions.  $N_{AFM}$  thus becomes another quantum number to break down the hamiltonian into more blocks.

For  $N_\uparrow = 3$ , there are three bands in the periodic chain, corresponding to configurations with (i) the three  $\uparrow$  spins next to each other ( $N_{AFM} = 2$ ), (ii) two  $\uparrow$ -spins neighboring each other and one disjoint ( $N_{AFM} = 4$ ), (iii) the three  $\uparrow$  spins all non-neighboring ( $N_{AFM} = 6$ ). In the open chain, the edge allows also configurations with odd  $N_{AFM}$  values; hence there are six bands. The total number of states in the  $N_\uparrow = 3$  sector is  $\binom{L}{3} = \frac{L(L-1)(L-2)}{6}$ . Table I collects the number of states in different bands for both open and closed chains, and lists corresponding  $N_{AFM}$  values. These counting arguments can be readily generalized to larger  $N_\uparrow$  sectors.

The band structure survives at finite but large anisotropies  $\Delta$ . Figure 1 illustrates this for a  $L = 10$  chain within the  $N_\uparrow = 3$  sector with  $\Delta = 10$ . Also shown here is the expectation value of  $\hat{N}_{AFM}$  as defined above; only an expectation value of this quantity can be computed for each eigenvector because the finite- $\Delta$  eigenstates of the Hamiltonian are not eigenstates of the operator  $\hat{N}_{AFM}$ . Nevertheless, the expectation value of  $\hat{N}_{AFM}$  remains close to the integer value expected for  $\Delta \rightarrow \infty$ , and there are sharp jumps across bands.

Figure 2 collects data for the open chain for a range of values of  $\Delta$ .  $\langle\hat{N}_{AFM}\rangle$  appears to be a rather sharp indicator of the band-structure, sometimes even sharper than energy itself.

### III. TOP TWO BANDS

The top two bands, corresponding to  $\langle\hat{N}_{AFM}\rangle \approx 1$  and to  $\langle\hat{N}_{AFM}\rangle \approx 2$ , were considered in Ref. [1]. Both have the same number of states for arbitrary  $N_\uparrow$ , namely 2, and  $L - 2$ . The application of the hopping ( $J_x$ ) terms does not lift the degeneracy of these two bands within first order-perturbation theory; thus the substructures of

$N_{AFM}$	Number of states(OBC)	Number of states(PBC)
1	2	-
2	$L-2$	$L$
3	$4(L-4)$	-
4	$(L-4)(L-4)$	$L(L-4)$
5	$(L-4)(L-5)$	-
6	$(L-4)(L-5)(L-6)/6$	$L(L-4)(L-5)/6$

TABLE I. The number of states belonging to different ‘bands’ at large  $\Delta$  within the  $N_\uparrow = 3$  sector. Each band being labeled by a value of  $N_{AFM}$ . The numbers sum to the total number of states in the full  $N_\uparrow = 3$  sector,  $\frac{L(L-1)(L-2)}{6}$ . There are only three bands for the closed chain, corresponding to  $N_{AFM} = 2, 4$ , and 6, and six bands for the open chain.

the  $\langle\hat{N}_{AFM}\rangle \approx 2$  only appear at higher order. We briefly review the physics of these bands here.

The top band is made of configurations where all  $N_\uparrow$  up-spins are at one edge. There are two states in this band because the up-spins can be pinned either to the left or the right edge. The separation of this band from the rest of the spectrum leads to the ‘trivial edge-locking’ physics described in Ref. [1]: a configuration like  $|\uparrow\uparrow\downarrow\downarrow\cdots\rangle$  will have very little dynamics at large  $\Delta$  as the  $\uparrow$ -block is locked to the edge.

The second band is composed of (a)  $\uparrow$ -spins in a single block away from the boundaries, (b) the  $\uparrow$ -spins separated into two blocks, each of them pinned to one of the edges of the chain. The band has substructures appearing at second and higher even orders in the hopping term; these lead to a ‘fractal’ structure in the spectrum and a corresponding set of nontrivial edge-locking phenomena [1].

### IV. THIRD BAND FROM THE TOP

In this section we will consider and explain the substructures seen in the third band from the top, corresponding to  $\langle\hat{N}_{AFM}\rangle \approx 3$  at large  $\Delta$ , for arbitrary  $N_\uparrow \leq L/2$ . We can only get configurations with  $N_{AFM} = 3$  provided the following constraints hold:

- The  $N_\uparrow$  up-spins appear in exactly two isolated blocks, with  $r$  and  $N_\uparrow - r$  up spins;  $r \in \{1, 2, \dots, (N_\uparrow - 1)\}$ .
- Either the left block sits at the left end of the chain, or the right block sits at the right end (but not both). We will refer to the two blocks as the ‘edge-pinned’ and ‘free’ blocks.

With these constraints, we can count that the number of states in the third band is  $2(N_\uparrow - 1)(L - N_\uparrow - 1)$ . For  $N_\uparrow = 3$ , this formula gives  $4(L - 4)$  which agrees with Table I.

Now, let us look at the substructure of this band. Figure 3 blows up the region around the third band for open

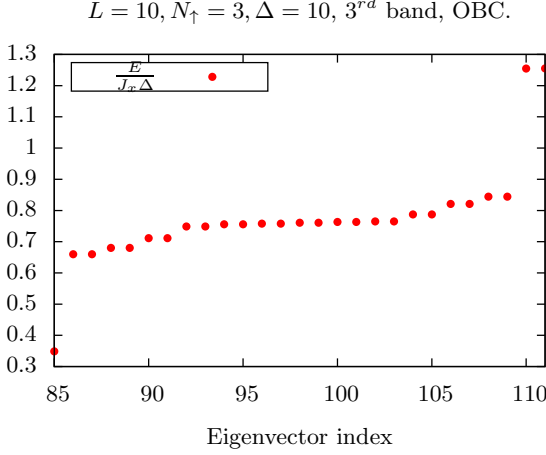


FIG. 3. Figure blows up the region around the third band of the spectrum for an open chain with size  $L = 10$ , and  $\Delta = 10$ , inside the  $N_\uparrow = 3$  sector. The  $4(L - 4) = 24$  states in this band run from 86 to 109.

chains of size  $L = 10$  for the  $N_\uparrow = 3$  sector. We see a central flat patch where a group of eigenstates are placed at roughly the same energies. On either side of this flat region, we find stairs with nearly degenerate pairs of eigenstates. We will next show that the substructure of this band for arbitrary  $N_\uparrow$  can be understood using first-order degenerate perturbation theory.

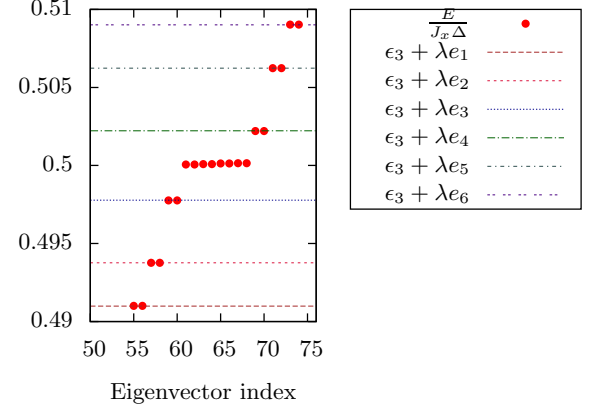
We start by rewriting the original Hamiltonian as

$$\frac{H}{J_x \Delta} = H_0 + \lambda H', \quad (3)$$

where  $H_0 = \sum_j S_j^z S_{j+1}^z$ ,  $H' = \sum_j S_j^x S_{j+1}^x + S_j^y S_{j+1}^y$ , and  $\lambda = 1/\Delta$ . We are interested in the third band from the top characterized by states with  $N_{AFM} = 3$  being dominant. When  $\lambda$  is precisely equal to zero, all the states in this band, regardless of  $N_\uparrow$ , have identical energy  $\epsilon_3 = (L-7)/4$  (in units of  $J_x \Delta$ ), because  $H_0$  depends only on  $N_{AFM}$ . Now, we turn on a tiny  $\lambda > 0$ . Exploiting standard degenerate perturbation theory, we recall that we must diagonalize the matrix  $W_{ij} = \langle \psi_i^0 | H' | \psi_j^0 \rangle$ , where  $|\psi_i^0\rangle$  are the  $2(N_\uparrow - 1)(L - N_\uparrow - 1)$  degenerate eigenstates that constitute the third band when  $\lambda = 0$ . This matrix nicely separates into two identical blocks, corresponding to whether the ‘pinned’ group of  $\uparrow$  spins is at the right edge or at the left edge. Being identical, these blocks give the same eigenvalues, and thus accounts for the occurrence of degenerate pairs in Fig.3. We will now concentrate on the eigenvalues of the block which has the left end ‘pinned’.

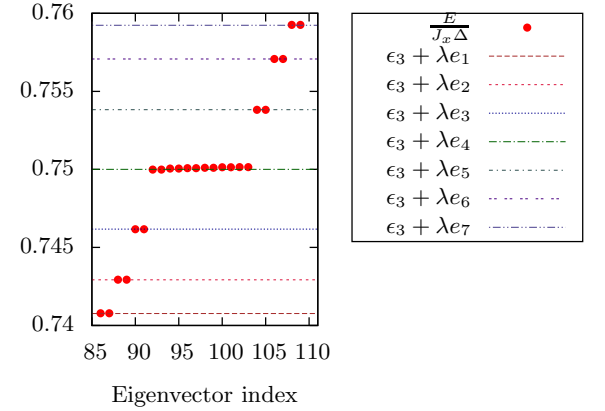
Among the ‘left-pinned’ states, only  $(L-3)$  states have first-order matrix elements. This is independent of  $N_\uparrow$ , so that the nonzero part of the  $W_{\text{left}}$  matrix is the same regardless of  $N_\uparrow$ . The remaining  $(N_\uparrow - 2)(L - N_\uparrow - 2)$  states give a large block of zeros at first order, and are responsible for the flat patch at the middle of the third

$L = 9, N_\uparrow = 3, \Delta = 100, \lambda = \frac{1}{\Delta} = 0.01, 3^{rd}$  band, OBC.



(a)

$L = 10, N_\uparrow = 3, \Delta = 100, \lambda = \frac{1}{\Delta} = 0.01, 3^{rd}$  band, OBC.



(b)

FIG. 4. Figure blows up the third band of the spectrum for an open chain with sizes  $L = 9$ , and  $L = 10$ , and  $\Delta = 100$  inside the  $N_\uparrow = 3$  sector. For  $L = 9$ , there are  $4(L-4) = 20$  in this band starting from 55 and going up until 74. For  $L = 10$ , the 24 states in this band run from 86 to 109, just like in Fig.3. Also included here are the analytical expectations for the energy levels from first-order degenerate PT,  $\epsilon_3 + \lambda e_r$ . We see that the analytical lines sit right on top of the numerical data points, showing that first-order PT is accurate for this value of  $\Delta$ . We also observe that for the even case  $L = 10$ , one of the energy levels falls at the ‘zero’, thus making the flat patch of length  $2(L-4) = 12$ . For the odd case of  $L = 9$ , the flat patch has length  $2(L-5) = 8$ .

band.

The states connected at first order by  $H'$  include the  $L - N_\uparrow - 1$  configurations where  $N_\uparrow - 1$  up-spins are edge-pinned and one is free, e.g., for  $N_\uparrow = 4$ , the states  $|\uparrow\uparrow\uparrow\downarrow\downarrow \cdots \downarrow\uparrow\downarrow\rangle$ ,  $|\uparrow\uparrow\uparrow\downarrow\downarrow \cdots \downarrow\uparrow\downarrow\downarrow\rangle$ ,  $|\uparrow\uparrow\uparrow\downarrow\downarrow \cdots \downarrow\uparrow\downarrow\downarrow\downarrow\rangle$ ,  $\cdots$ ,  $|\uparrow\uparrow\uparrow\downarrow\uparrow\downarrow \cdots \downarrow\rangle$ . Any two successive pairs of these are connected by  $H'$ . Successive application of  $H'$  on the last of these states connects also configurations with smaller numbers  $N_\uparrow - r$  of edge-pinned spins (one for each  $r > 1$ ). In the  $N_\uparrow = 4$  case, these are  $|\uparrow\uparrow\downarrow\uparrow\uparrow\downarrow \cdots \downarrow\rangle$  and  $|\uparrow\downarrow\uparrow\uparrow\uparrow\downarrow \cdots \downarrow\rangle$ . There are  $N_\uparrow - 2$  such states. So the

total number of states that give a non-zero block in  $W_{\text{left}}$  is  $L - N_{\uparrow} - 1 + N_{\uparrow} - 2 = L - 3$ , independent of  $N_{\uparrow}$ . We write the  $(L - 3) \times (L - 3)$  dimensional matrix  $W_{\text{left}}$ :

$$W_{\text{left}} = \begin{pmatrix} 0 & \frac{1}{2} & 0 & \cdots & 0 & 0 & 0 \\ \frac{1}{2} & 0 & \frac{1}{2} & 0 & \cdots & 0 & 0 \\ 0 & \frac{1}{2} & 0 & \frac{1}{2} & 0 & \cdots & 0 \\ \vdots & & & & & & \\ 0 & 0 & \cdots & 0 & \frac{1}{2} & 0 & \frac{1}{2} \\ 0 & 0 & \cdots & 0 & 0 & \frac{1}{2} & 0 \end{pmatrix}, \quad (4)$$

However this is a well-studied type of matrix in the literature [8] called 1-Toeplitz matrix, whose eigenvalues are given by:

$$e_r = -\cos\left(\frac{r\pi}{L-2}\right), \quad r = 1, 2, \dots, (L-3). \quad (5)$$

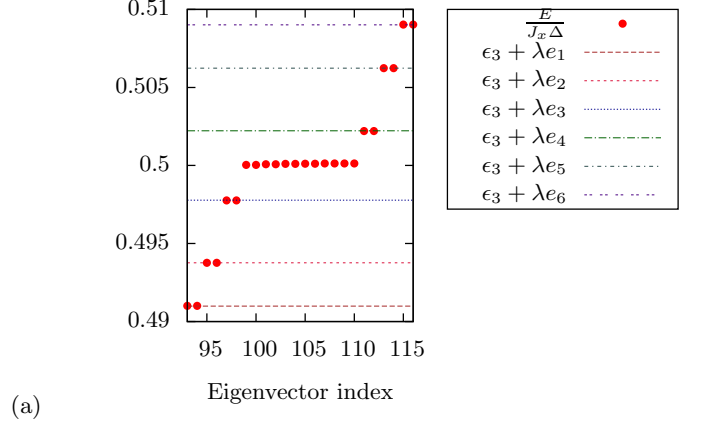
When  $L$  is even, a zero eigenvalue appears because of  $\cos \frac{\pi}{2}$ , thus this accounts for the extra pair in the flat patch we see for the case of  $L = 10$ , sector  $N_{\uparrow} = 3$  in Fig.3. In order to show this even more clearly, and to show that the above analysis fits perfectly with the numerics, we show in Fig.4 the third band for sizes  $L = 9$ , and  $L = 10$ , for the  $N_{\uparrow} = 3$ -sector, with a large  $\Delta = 100$ . Simultaneously, we show the energies obtained analytically above as  $\epsilon_3 + \lambda e_r$ . We see that the analytical energies sit right on top of the numerically computed ones. We also observe that the central flat patch is of length  $2(L - 4)$  for even  $L$  because of the presence of a zero eigenvalue of the matrix  $W$ , whereas it is only  $2(L - 5)$  for odd  $L$ .

In order to show the generality of our result, we show in Fig.5 the third band for sizes  $L = 9$ , and  $L = 10$ , for the  $N_{\uparrow} = 4$  sector, with a large  $\Delta = 100$ . Simultaneously, we show the energies obtained analytically above as  $\epsilon_3 + \lambda e_r$ . We see that the analytical energies sit right on top of the numerically computed ones. We also observe that the central flat patch is of length  $2((N_{\uparrow} - 2)(L - N_{\uparrow} - 2) + 1)$  for even  $L$  because of the presence of a zero eigenvalue of the matrix  $W$ , whereas it is only  $2(N_{\uparrow} - 2)(L - N_{\uparrow} - 2)$  for odd  $L$ .

## V. PROPAGATION DYNAMICS

Having analyzed the structure of the states making up the third band from the top ( $\langle \hat{N}_{AFM} \rangle \approx 3$  band), we can explore some dynamical consequences (Figure 6). Considering the  $N_{\uparrow} = 3$  case, we have found that all but one of the configurations with one  $\uparrow$  spin edge-pinned are part of the flat manifold due to having no matrix elements at leading order. The exception is the state  $|\uparrow\uparrow\uparrow\downarrow\downarrow\dots\rangle$ , i.e., the configuration where the ‘free’ group of  $N_{\uparrow} - 1$  spins sits at minimum distance from the edge-pinned part. This configuration is part of the nonzero  $W$  matrix constructed in the last section, and hybridizes at first order with the configurations where a single  $\uparrow$

$L = 9, N_{\uparrow} = 4, \Delta = 100, \lambda = \frac{1}{\Delta} = 0.01, 3^{rd}$  band, OBC.



$L = 10, N_{\uparrow} = 4, \Delta = 100, \lambda = \frac{1}{\Delta} = 0.01, 3^{rd}$  band, OBC.

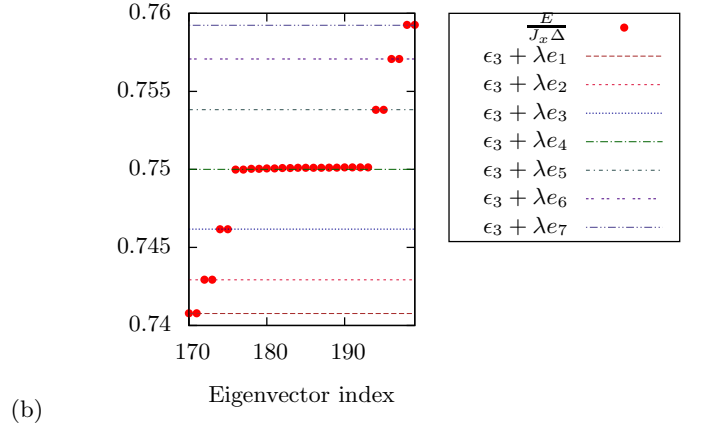


FIG. 5. Figure blows up the third band of the spectrum for an open chain with sizes  $L = 9$ , and  $L = 10$ , and  $\Delta = 100$  inside the  $N_{\uparrow} = 4$  sector. For  $L = 9$ , there are  $6(L - 5) = 24$  states in this band starting from 93 and going up until 116. For  $L = 10$ , the  $6(L - 5) = 30$  states in this band run from 170 to 199. Also included here are the analytical expectations for the energy levels from first-order degenerate PT,  $\epsilon_3 + \lambda e_r$ . We see that the analytical lines sit right on top of the numerical data points, showing that first-order PT is accurate for this value of  $\Delta$ . We also observe that for the even case  $L = 10$ , one of the energy levels falls at the ‘zero’, thus making the flat patch of length  $2(2(L - 6) + 1) = 18$ . For the odd case of  $L = 9$ , the flat patch has length  $2(2(L - 6)) = 12$ .

spin is free. This implies, for example, that open chains initiated with states

$$|\alpha\rangle = |\uparrow\downarrow\uparrow\downarrow\downarrow\dots\rangle \text{ and } |\beta\rangle = |\uparrow\downarrow\downarrow\uparrow\downarrow\dots\rangle \quad (6)$$

should have qualitatively different dynamics; the first can propagate by first-order hopping processes and the second cannot.

Figure 6, top panel, displays this difference. Starting with the initial state  $|\alpha\rangle$ , the ‘free’ block transfers ( $N_{\uparrow} - 2 = 1$ ) of its members to the edge-pinned block, after which the remaining single free  $\uparrow$  spin propagates at the

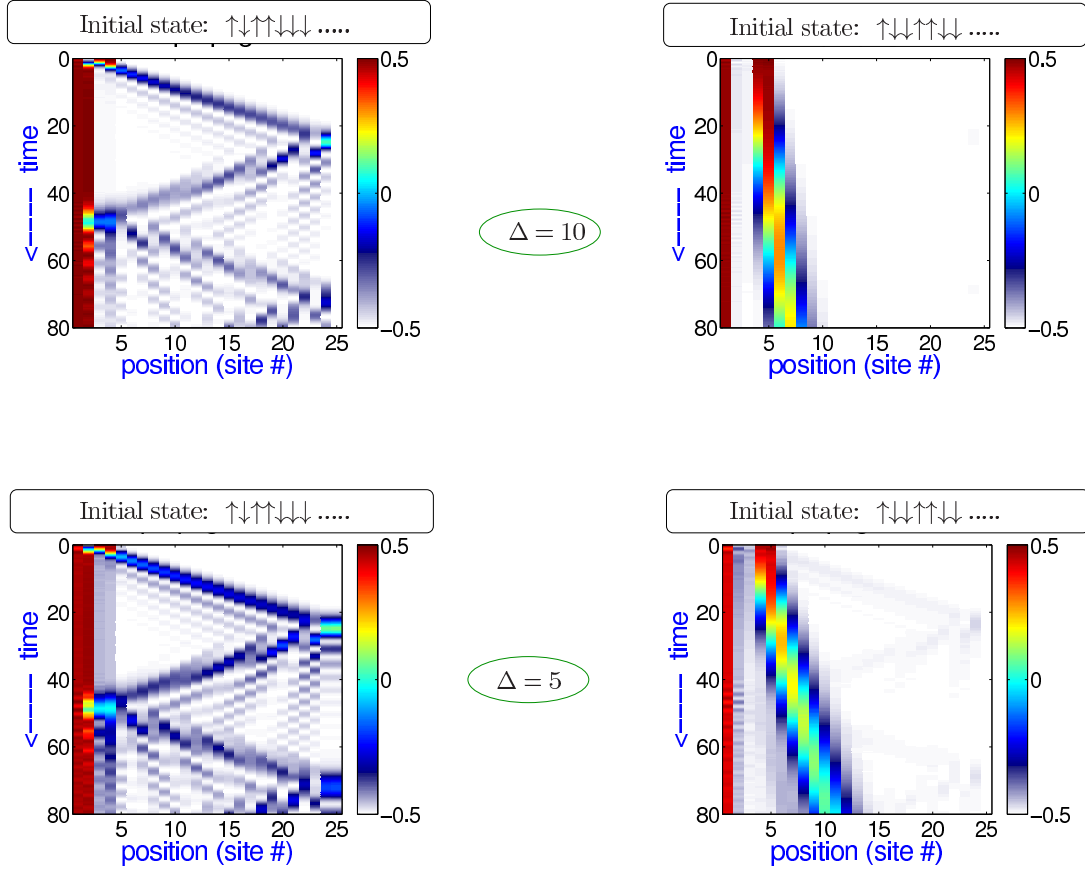


FIG. 6. Time evolution for chains initiated with configurations  $|\alpha\rangle$  (left column) and  $|\beta\rangle$  (right column), as defined in Equation (6). Two values of the anisotropy  $\Delta$  are compared for each initial state (top and bottom rows).

typical magnon velocity,  $J_x$  [9]. With the initial state  $|\beta\rangle$ , however, the dynamics does not significantly access the "single-free-spin" sector; therefore the propagation is through higher-order processes; the non-edge-pinned part moves as a bound bi-magnon at slower speeds [9].

The bottom panel shows data for a smaller  $\Delta$ ; the bi-magnon speed is larger. There is greater admixture between the sectors separated at first order, therefore there is some probability for single-magnon propagation also with the  $|\beta\rangle$  initial state.

## VI. FOURTH BAND FROM THE TOP

Next we will consider the fourth band from the top, corresponding to  $\langle \hat{N}_{AFM} \rangle \approx 4$  at large  $\Delta$ . It is obvious that  $N_\uparrow = 1$  cannot give rise to this band, so we need at least  $N_\uparrow = 2$ . The  $N_\uparrow = 2$  case however turns out to be pathological, and perhaps not even analytically tractable, so we relegate a discussion of this to the end of this section. For  $3 \leq N_\uparrow \leq L/2$ , we can only get configurations with  $N_{AFM} = 4$  in one of the following two ways:

- (a) There are three isolated groups of contiguous-up-spins, one which is pinned to the left end, the

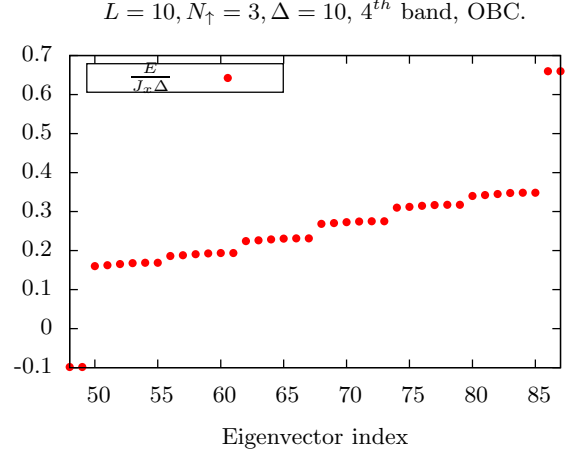


FIG. 7. Figure blows up the region around the fourth band of the spectrum for an open chain with size  $L = 10$ , and  $\Delta = 10$  inside the  $N_\uparrow = 3$  sector. There are  $(L-4)(L-4) = 36$  states in this band starting from 50 and going up until 85.

other to the right end, and one in between them.

- (b) There are two isolated groups of contiguous-up-

spins, neither of which is pinned to an end.

To count the number of ways of doing case (a), let us say there are  $r$  up-spins on the left end, and  $s$  up-spins on the right end (with  $r \geq 1, s \geq 1$ ), and  $t$  up-spins in between, such that  $r + s + t = N_\uparrow$ . Clearly, the number of ways of choosing  $r$  and  $s$  is  $\binom{N_\uparrow-1}{2} = \frac{(N_\uparrow-1)(N_\uparrow-2)}{2}$ . For each of these ways of choosing  $r, s$ , there are  $L - N_\uparrow - 1$  ways of putting the central block of  $t$ -up-spins. Thus there are  $\frac{(N_\uparrow-1)(N_\uparrow-2)(L-N_\uparrow-1)}{2}$  states of type (a). In order to count the number of ways of doing case (b), we first observe that there are  $(N_\uparrow - 1)$  ways in which the number of up-spins can be divided between the two groups. For each of these ways of division, there are  $\frac{(L-2-N_\uparrow)(L-1-N_\uparrow)}{2}$  of positioning the two groups in the available  $L - 2$  spots. Thus the total number of states of type (b) is  $\frac{(N_\uparrow-1)(L-2-N_\uparrow)(L-1-N_\uparrow)}{2}$ . Therefore, the total number of states in this band is  $\frac{(N_\uparrow-1)(L-N_\uparrow-1)(L-4)}{2}$ .

Now, let us look at the substructure of this band. Fig. 7 blows up the region around the fourth band for system-size  $L = 10$  with  $N_\uparrow = 3$ . We see that there are  $(L - 4)$  subbands each containing  $(L - 4)$  states.

Motivated by the success with the third band, we now ask if this substructure can be precisely understood with the help of first-order degenerate perturbation theory. Again, we start by rewriting the original Hamiltonian as

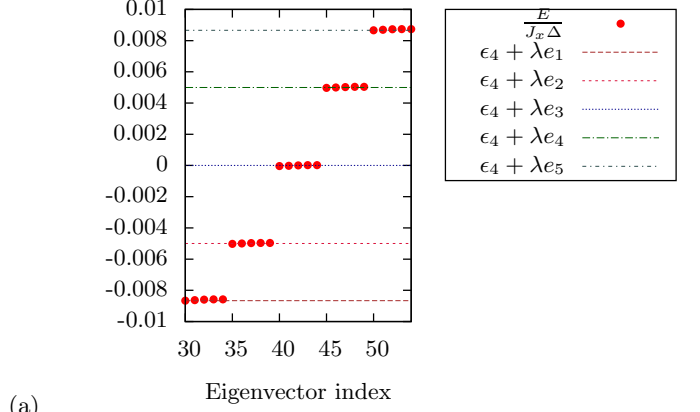
$$\frac{H}{J_x \Delta} = H_0 + \lambda H', \quad (7)$$

where  $H_0 = \sum_j S_j^z S_{j+1}^z$ ,  $H' = \sum_j S_j^x S_{j+1}^x + S_j^y S_{j+1}^y$ , and  $\lambda = 1/\Delta$ , with particular focus on the the fourth band from the top characterized by states with  $N_{AFM} = 4$  being dominant. When  $\lambda$  is precisely equal to zero, all the states in this band, regardless of  $N_\uparrow$  have identical energy  $\epsilon_4 = (L - 9)/4$  (in units of  $J_x \Delta$ ), which agrees with Fig. 7. Again, we have the task of diagonalizing the matrix  $W_{ij} = \langle \psi_i^0 | H | \psi_j^0 \rangle$ , where  $|\psi_i^0\rangle$  are the  $\frac{(N_\uparrow-1)(L-N_\uparrow-1)(L-4)}{2}$  degenerate eigenstates that constitute the fourth band when  $\lambda = 0$ . Let us denote a generic  $m \times m$  1-Toeplitz matrix of the type we encountered in the last section by  $T_m$ . That is,

$$T_m = \begin{pmatrix} 0 & \frac{1}{2} & 0 & \cdots & 0 & 0 & 0 \\ \frac{1}{2} & 0 & \frac{1}{2} & 0 & \cdots & 0 & 0 \\ 0 & \frac{1}{2} & 0 & \frac{1}{2} & 0 & \cdots & 0 \\ \vdots & & & & & & \\ 0 & 0 & \cdots & 0 & \frac{1}{2} & 0 & \frac{1}{2} \\ 0 & 0 & \cdots & 0 & 0 & \frac{1}{2} & 0 \end{pmatrix}, \quad (8)$$

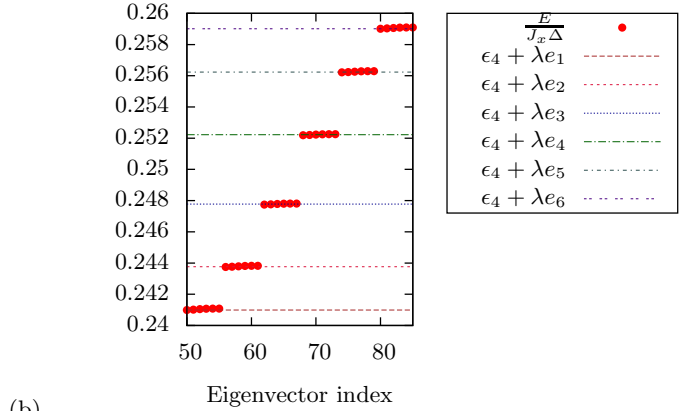
where it is understood that the  $m$  in  $T_m$  means there are  $m$  columns and  $m$  rows. It turns out that the matrix  $W$  can entirely be written as blocks of  $T_m$ , and it is independent of  $N_\uparrow$ . We show explicitly the ordering of states that leads to this structure for the simplest non-trivial case,  $N_\uparrow = 4$ , and then the generalization to arbitrary  $N_\uparrow$  is

$L = 9, N_\uparrow = 3, \Delta = 100, \lambda = \frac{1}{\Delta} = 0.01, 4^{th}$  band, OBC.



(a)

$L = 10, N_\uparrow = 3, \Delta = 100, \lambda = \frac{1}{\Delta} = 0.01, 4^{th}$  band, OBC.



(b)

FIG. 8. Figure blows up the fourth band of the spectrum for an open chain with sizes  $L = 9$ , and  $L = 10$ , and  $\Delta = 100$  inside the  $N_\uparrow = 3$  sector. For  $L = 9$ , there are  $(L-4)(L-4) = 25$  states in this band starting from 30 and going up until 54. For  $L = 10$ , the 36 states in this band run from 50 to 85, just like in Fig. 7. Also included here are the analytical expectations for the energy levels from first-order degenerate PT,  $\epsilon_4 + \lambda e_r$ . We see that the analytical lines sit right on top of the numerical data points, showing that first-order PT is accurate for this value of  $\Delta$ . We also observe that for the odd case  $L = 9$ , one of the energy levels falls at the 'zero', thus leaving some states unchanged in energy. For the even case of  $L = 10$ , all the states have a different energy even at the slightest of perturbations.

obvious. We first observe that states of type (a) and type (b) do not mix and naturally separate into blocks. Next we look at the states of the type (a) grouped together as  $|\uparrow\uparrow\downarrow\downarrow \cdots \downarrow \cdots \uparrow\uparrow\rangle, |\uparrow\downarrow\uparrow\downarrow \cdots \downarrow \cdots \uparrow\uparrow\rangle, \dots, |\uparrow\downarrow \cdots \uparrow\uparrow\uparrow\rangle, |\uparrow\downarrow \cdots \uparrow\uparrow\downarrow\rangle$ . It is clear that this group of states just gives an independent  $(L - 4) \times (L - 4)$  dimensional block given by  $T_{(L-4)}$ . Again, we could do the same type of ordering of states starting with the left end having 2 up-spins and the right end having 1. Again we will get another  $(L - 4) \times (L - 4)$  dimensional block



given by  $T_{(L-4)}$ . Similarly we could do this starting with any  $r$  up-spins on the left end, and any  $N_\uparrow - 1 - r$  up-spins on the right end, leaving one-up-spin which can travel across. Some thought reveals that for arbitrary  $N_\uparrow$ , the states of type (a) can be grouped in such a way as to give  $(N_\uparrow - 2)$  blocks of  $T_{(L-4)}$ . All the other states which do not participate in these blocks do not contribute. Now, within the states of the type (b) above, if we group the states  $|\downarrow\uparrow\uparrow\downarrow\downarrow\cdots\uparrow\downarrow\rangle, |\downarrow\uparrow\uparrow\downarrow\downarrow\cdots\uparrow\downarrow\downarrow\rangle, \dots, |\downarrow\uparrow\uparrow\downarrow\downarrow\downarrow\cdots\downarrow\rangle, |\downarrow\uparrow\uparrow\downarrow\downarrow\downarrow\cdots\downarrow\rangle, |\downarrow\uparrow\uparrow\downarrow\downarrow\downarrow\cdots\downarrow\rangle$ , they form the independent  $(L-4) \times (L-4)$  dimensional block given by  $T_{(L-4)}$ . Similarly, the group of states  $|\downarrow\downarrow\uparrow\uparrow\downarrow\downarrow\cdots\uparrow\downarrow\rangle, |\downarrow\downarrow\uparrow\uparrow\downarrow\downarrow\cdots\uparrow\downarrow\downarrow\rangle, \dots, |\downarrow\downarrow\uparrow\uparrow\downarrow\downarrow\downarrow\cdots\downarrow\rangle, |\downarrow\downarrow\uparrow\uparrow\downarrow\downarrow\downarrow\cdots\downarrow\rangle, |\downarrow\downarrow\uparrow\uparrow\downarrow\downarrow\downarrow\cdots\downarrow\rangle$  form another independent  $(L-4) \times (L-4)$  dimensional block given by the same  $T_{(L-4)}$ . Some inspection reveals that all the contributing states of type (b) can similarly be grouped into suitable blocks of  $(L-4)$  states; since there are  $(L - N_\uparrow - 2)$  such blocks, this leads to  $(L - N_\uparrow - 2)$  blocks of  $T_{(L-4)}$ . Therefore, we now see that the full  $W$  matrix is composed of  $N_\uparrow - 2 + L - N_\uparrow - 2 = (L - 4)$  blocks of  $T_{(L-4)}$ . Quite remarkably, a large number of states give zero-blocks thus reducing a  $(\frac{(N_\uparrow-1)(L-N_\uparrow-1)(L-4)}{2}) \times (\frac{(N_\uparrow-1)(L-N_\uparrow-1)(L-4)}{2})$  matrix to just an  $(L-4)^2 \times (L-4)^2$  matrix independent of  $N_\uparrow$ . The matrix  $W$  is:

$$W = \begin{pmatrix} T_{(L-4)} & 0 & 0 & \cdots & 0 & 0 & 0 \\ 0 & T_{(L-4)} & 0 & 0 & \cdots & 0 & 0 \\ 0 & 0 & T_{(L-4)} & 0 & 0 & \cdots & 0 \\ \vdots & & & & & & \\ 0 & 0 & \cdots & 0 & 0 & T_{(L-4)} & 0 \\ 0 & 0 & \cdots & 0 & 0 & 0 & T_{(L-4)} \end{pmatrix}. \quad (9)$$

Therefore once again using the well-known results of 1-Toeplitz matrices [8], we have that the eigenvalues of  $W$  are

$$e_r = -\cos\left(\frac{r\pi}{L-3}\right), \quad r = 1, 2, \dots, (L-4), \quad (10)$$

with each eigenvalue being  $(L-4)$  times degenerate. So, the energies of the sub-bands of the fourth band should be given by  $\epsilon_4 + \lambda e_r$ . In order to compare this result with numerics, in Fig.8, we show data for a run inside the  $N_\uparrow = 3$  sector, with a very large value of  $\Delta = 100$ , for which one expects first-order perturbation theory to hold. The agreement between the numerical exact diagonalization and the analytical expectation is perfect. It is worth pointing out here that for  $N_\uparrow = 3$ ,  $\frac{(N_\uparrow-1)(L-N_\uparrow-1)(L-4)}{2} = (L-4)^2$ , therefore, the  $W$  matrix does not have an explicit zeros block. Hence, in Fig. 8, we see unperturbed states only when  $L$  is odd, and the number of these is  $(L-4)$ , one from each of the 1-Toeplitz matrices in  $W$  according to Eq. (10). When  $N_\uparrow > 3$ , we would see a central unperturbed patch of length  $\frac{(N_\uparrow-3)(L-N_\uparrow-3)(L-4)}{2}$  for all values of  $L$ , and additional  $(L-4)$  unperturbed states when  $L$  is odd.

Now we briefly discuss the pathological  $N_\uparrow = 2$  case. It is obvious that only states of type (b) occur here. Barring states where one or both of the up-spins occupies the penultimate position from either end, every state typically has a non-zero overlap with four states since each of the two up-spins could move either to the left or to the right. Therefore, a typical row of the  $W$  matrix has 4 elements which are 1/2 with all others being zero. Thus already the 1-Toeplitz structure is lost; in addition there is also the complication of states where one or both of the up-spins may have mobility curtailed, which will lead to some rows having less than 4 non-zero elements. We are not aware of a simple analytic expression for the eigen-spectrum of this matrix. It is worth noting here that for  $N_\uparrow = 2$ , the fourth band is the ‘last’ band (fifth and sixth bands don’t exist); thus, it is not a surprise that it is pathological.

## VII. BANDS FARTHER FROM THE TOP

The bands farther down in the spectrum have less pronounced structure. For the  $\langle \hat{N}_{AFM} \rangle \approx 5$  band, degenerate perturbation theory at first order leads to a complicated degeneracy matrix which is similar to that encountered in the pathological  $N_\uparrow = 2$  case of the fourth band; numerical diagonalization of this matrix reproduces the actual spectrum at large  $\Delta$ , but we were unable to obtain simple analytic expressions, or a simple description of the substructures.

## VIII. CONCLUSIONS

We studied band structures and substructures in the open-boundary Heisenberg chain at large anisotropy, using degenerate perturbation theory to explain the most prominent features. We also presented real-time evolution phenomena reflecting these spectral structures.

The features of the spectrum we have examined relate in particular to the propagation and binding of magnons and collections of magnons in a ferromagnetic background. The study of this type of non-equilibrium situations is of growing current interest [3, 9–11]. The intriguing possibility of controlling such propagation phenomena using geometric features like edges and impurities deserves further exploration; our dynamics results in Section V is just one such example.

Our work also raises several other questions, e.g., are there generic ways in which the spectral structures get modified at smaller  $\Delta$ ? It is also an open question how the intricate spectral structures get modified or destroyed if we have a weak bond rather than a fully open-boundary chain; one can interpolate between periodic and open-boundary cases by weakening one of the bonds in a periodic chain.

*Acknowledgments.* AS thanks S. Ramasesha for valuable discussions, and a careful reading of the manuscript.



- 
- [1] M. Haque, Phys. Rev. A **82**, 012108 (2010).
  - [2] T. Fukuhara, A. Kantian, M. Endres, M. Cheneau, P. Schauß, S. Hild, D. Bellem, U. Schollwöck, T. Giamarchi, C. Gross, I. Bloch, and S. Kuhr, Nature Physics **9**, 235 (2013).
  - [3] T. Fukuhara, P. Schauß, M. Endres, S. Hild, M. Cheneau, I. Bloch, and C. Gross, arXiv:1305.6598.
  - [4] C. Gross and I. Bloch, private communication.
  - [5] A. Lyakhov and C. Bruder, New J. Phys. **7**, 181 (2005 ).
  - [6] L.-M. Duan, E. Demler, and M. D. Lukin, Phys. Rev. Lett. **91**, 090402 (2003).
  - [7] A. Kay and D. G. Angelakis, Europhys. Lett. **84**, 20001 (2008).
  - [8] M. Gover, *Linear Algebra and its Applications*, **197**, 63 (1994).
  - [9] M. Ganahl, E. Rabel, F. H. L. Essler, and H. G. Evertz, Phys. Rev. Lett. **108**, 077206 (2012).
  - [10] M. Ganahl, M. Haque, and H. G. Evertz, arXiv:1302.2667
  - [11] A. Wöllert and A. Honecker, Phys. Rev. B **85**, 184433 (2012).